The Astrophysical Journal, 774:140 (8pp), 2013 September 10 doi:10.1088/0004-637X/774/2/140

A STATISTICAL STUDY OF THE SPECTRAL HARDENING OF CONTINUUM EMISSION IN SOLAR FLARES

X. Kong[1,2], G. Li[2], and Y. Chen[1]
[1] Institute of Space Sciences and School of Space Science and Physics, Shandong University, Weihai 264209, China; xl_kong@hotmail.com
[2] Department of Physics and CSPAR, University of Alabama in Huntsville, Huntsville, AL 35899, USA; gang.li@uah.edu
Received 2013 March 26; accepted 2013 July 22; published 2013 August 26

ABSTRACT

The observed hard X-ray and γ-ray continuum in solar flares is interpreted as Bremsstrahlung emission of accelerated non-thermal electrons. It has been noted for a long time that in many flares the energy spectra show hardening at energies around or above 300 keV. In this paper, we first conduct a survey of spectral hardening events that were previously studied in the literature. We then perform a systematic examination of 185 flares from the Solar Maximum Mission. We identify 23 electron-dominated events whose energy spectra show clear double power laws. A statistical study of these events shows that the spectral index below the break (γ_1) anti-correlates with the break energy (ε_b). Furthermore, γ_1 also anti-correlates with Fr, the fraction of photons above the break compared to the total photons. A hardening spectrum, as well as the correlations between (γ_1, ε_b) and (γ_1, Fr), provide stringent constraints on the underlying electron acceleration mechanism. Our results support a recent proposal that electrons are being accelerated diffusively at a flare termination shock with a width of the order of an ion inertial length scale.

Key words: acceleration of particles – Sun: flares – Sun: particle emission – Sun: X-rays, gamma rays

Online-only material: color figures

1. INTRODUCTION

Solar Energetic Particle (SEPs) are often caused by Coronal Mass Ejections (CMEs) and solar flares, the two most energetic phenomena in the solar system. During solar flares, electrons can be accelerated to energies as high as hundreds of mega-electronvolts (MeV) and ions can reach energies of tens of gigaelectronvolts (GeV). Hard X-ray (HXR) and γ-ray continuum emission is known to be generated from non-thermal electrons through electron-ion Bremsstrahlung when electrons collide with the ambient plasma. The analysis of flare spectra provides valuable information on particle acceleration models as well as the physics of the background plasma in the solar corona and chromosphere (see recent reviews, Lin 2011; Fletcher et al. 2011; Holman et al. 2011; Kontar et al. 2011).

In studying SEP events, features such as spectral breaks are often used to obtain detailed information on the underlying acceleration process. For example, in gradual SEP events where protons and ions are accelerated at shocks driven by CMEs, Li et al. (2009) showed that by examining how the spectral break location varies as a function of the charge-to-mass ratio, one can infer the shock geometry at the acceleration site. In the case of solar flares, features in the continuum spectrum also reveal valuable information about the flaring process. Typically, the HXR energy spectrum is forward-fitted with a single or double power law (with a downward break at tens of keV) spectrum of source electrons. At higher energies, above the emission in the γ-ray range ($\sim$300 keV), additional physical processes including electron–positron annihilation at 0.511 MeV, neutron capture at 2.223 MeV, nuclear de-excitation from energetic ions, pion decay, inverse Compton scattering, electron–electron Bremsstrahlung, etc. (Vestrand 1988; Aschwanden 2004; Vilmer et al. 2011; Chen & Bastian 2012; Kontar et al. 2007), contribute to the total observed spectrum. Rieger & Marschhäuser (1990) reported a class of γ-ray flares that exhibits little or no evidence of nuclear γ-ray lines, the so-called electron-dominated events. Since then, many more electron-dominated events have been observed (e.g., Trottet et al. 1998; Vilmer et al. 1999; Rieger et al. 1998; Yoshimori et al. 1992). In these events, electron Bremsstrahlung emission dominates and one can therefore infer the source electron spectrum from the continuum spectrum.

An intriguing observation in many flares, including but not confined to the electron-dominated events, is the hardening of the flare continuum spectrum at energies often higher than 300 keV. For example, spectral hardening has been reported in many flares from the *Reuven Ramaty High Energy Spectroscopic Imager* (*RHESSI*; Lin et al. 2003; Share et al. 2003; Share & Murphy 2006; Shih et al. 2009) and *Fermi* observations (Ackermann et al. 2012). In an earlier work, Suri et al. (1975) examined a γ-ray flare event on 1974 August 4 using an γ-ray detector on the *Seventh Orbiting Solar Observatory* (*OSO-7*) satellite. These authors noted a change in the spectral shape at $\sim$700 keV and argued that the hardening was real and not artificial and that it must have been produced by Bremsstrahlung from a spectrum of non-thermal electrons showing a hardening feature.

A spectrum hardening at high energies is not easy to explain. One natural explanation is that there are two populations of emission: one dominating at low energies with a softer spectrum and the other dominating at high energies with a harder spectrum. These two populations need not to be spatially coincident. For example, using *RHESSI*, Krucker et al. (2008) examined the 2005 January 20 event and found that the footpoint source had a softer spectrum and the coronal source had a harder spectrum. Note that if there are spatially separated sources (looptop and footpoints) of continuum emission, then the hardening of the continuum does not necessarily imply a hardening of the source electron spectrum. For example, by assuming the emission is a sum of both thin-target emission from trapped electrons at the acceleration site near the looptop and thick target emission from escaping electrons precipitating on the solar surface, and noting that electrons with lower energies have shorter escape times due to the energy dependence of the Bremsstrahlung cross section differing in the nonrelativistic and the relativistic regimes, Park et al. (1997) were able to account

Table 1
Spectral Hardening Events in the Literature

Event No.	Date	Photon Spectrum			Spacecraft	Electron-dominated (Y/N)	Reference
		γ_1	γ_2	ε_b (MeV)			
1	1967 May 23	3.2	1.2	0.6	*ERS-18*		Gruber et al. (1973)
2	1972 Aug 4	3.4	1.7	0.7	*OSO-7*		Suri et al. (1975)
3	1981 Apr 1	3.75		0.4	*Hinotori*		Yoshimori et al. (1985)
4	1981 Apr 4	3.28		0.4	–		–
5	1981 Apr 27	4.0		0.4	–		–
6	1981 May 13	3.22		0.4	–		–
7	1990 Jun 11	4.0	2.0	0.35	*GRANAT*	Y	Trottet et al. (1998)
	Peak c	4.4	2.0	0.36	–	–	–
	Peak d	2.9	1.7	0.74	–	–	–
	Peak e	4.2	2.0	0.38	–	–	–
8	1991 Jun 30	2.8	1.9	0.54	*GRANAT*	Y	Vilmer et al. (1999)
		2.8	1.75	0.58	*CGRO*	–	–
9	1991 Dec 3	4.06	2.66	0.4	*Yohkoh*	Y	Yoshimori et al. (1992)
10	1980 Jun 4	4.3	2.2	0.3	*SMM*	Y	Dennis (1988)
11	2002 Jul 23	2.92	2.11	0.53	*RHESSI*	N	Share et al. (2003)
12	2003 Oct 28	3.8	2.1	0.46	*RHESSI*	N	Share & Murphy (2006)
13	2005 Jan 20	2.9	1.5	0.45	*RHESSI*	N	Krucker et al. (2008)
14	2010 Jun 12	3.31	1.2	1.3	*Fermi*	N	Ackermann et al. (2012)
15		2.73	1.84	1.0	*SMM*	Y	Rieger et al. (1998)

for the observed spectral hardening around 1 MeV for four flares.

In the work of Park et al. (1997), the source electron was assumed to be a single power law. In contrast, another explanation for the spectral hardening of the continuum emission is that the hardening reflects an intrinsic hardening in the source (Bremsstrahlung-emitting) electron spectrum (Dennis 1988; Yoshimori 1985; Yoshimori et al. 1992). Such an explanation is somewhat supported by early in situ observations. Indeed, Moses et al. (1989) examined 55 events using *ISEE 3 (ICE)* and found that a hardening of the electron spectrum was rather common in short duration (<1 hr for soft X-rays) events. Assuming these in situ electrons are the source electrons escaping from the acceleration site through, for example, interchange reconnection, the results of Moses et al. (1989) suggest that the accelerated electron population has a hardening at high energies.

High-energy electrons with energies greater than several hundred of keV can also produce microwave emission via gyrosynchrotron radiation. Combined analysis of HXRs and microwaves reveal that the electron energy distribution inferred from the microwave spectrum is harder than that from the HXR spectrum; this result suggests an intrinsic spectral hardening for the source electron spectrum around several hundred keV (e.g., Silva et al. 2000; Asai et al. 2013). On the other hand, in a recent study by Kawate et al. (2012), these authors concluded that electrons responsible for HXRs and microwaves have a common energy distribution and that the hardening of microwave emission is due to a more efficient trapping of electrons with higher energies. In this work, we do not consider the microwave emission and focus only on the HXR and γ-ray emission produced by the Bremsstrahlung process.

Limb events with occulted footpoints are helpful in discriminating these two different scenarios since in these events only the coronal source can be detected. In a recent work, Krucker et al. (2010) examined an east limb event that occurred on 2007 December 31. These authors found that the >30 keV source lay on top of the flare (but was elongated along the flare ribbon) and could be fit by a single power law with a spectral index of $\gamma \sim 4.2 \pm 0.1$, which translates to $\delta_e \sim 3.7 \pm 0.1$, assuming a thin target model. In comparison, the microwave observations at the same time yielded a slightly harder spectrum with $\delta_\mu \sim 3.4$. Therefore, there is no significant hardening in the 2007 December 31 event. Note that this event was a short-duration event. However, because it was an east limb event, no near-earth observations were available.

Furthermore, because the decay phase of the emission for the looptop and footpoints is very different (i.e., the looptop source will dominate at late stages; Krucker et al. 2008), examining the time evolution of the HXR spectrum in a flare, and in particular the relative intensities below and above the break, may also offer some checks for these two scenarios.

In this work, we assume that the hardening in the continuum is caused by an intrinsic hardening in the source electron. In our recent study (Li et al. 2013), we suggested that hardening in an electron spectrum at high energies can be obtained by the diffusive shock acceleration of electrons at a flare termination shock that has a finite width on the order of an ion inertial length scale. The accelerated electrons are likely the heated electrons during the flare process, but can also be electrons accelerated previously. One necessary condition for the proposed scenario is that high-energy electrons resonate with the inertial range of the magnetohydrodynamics (MHD) turbulence and low-energy electrons resonate with the dissipation range of the MHD turbulence. A further condition is that the turbulence spectrum is in the dissipation range $\sim k^{-2.7}$. Li et al. (2013) also performed numerical simulations with momentum-dependent diffusion coefficients and showed that the accelerated electron spectrum can develop hardenings comparable to observations.

As a continuation of Li et al. (2013), we conduct a statistical study of electron-dominated events that show clear spectral hardenings. Except for a few events from the literature (see Table 1), most events we considered are time-integrated spectra averaged over the entire flare. Considering that time-integrated spectra can minimize the effect of trapping since the trapping (at least in the simplest scenario) does not change the energy of an electron, and therefore a spectral hardening cannot be produced by trapping alone.

Table 2
The 23 Spectral Hardening Events Selected from Vestrand et al. (1999)

Event No.	Date	Time (UT)	Photon Spectrum γ_1	γ_2	ε_b (MeV)	$N(\varepsilon_b)$ (s^{-1} MeV^{-1})	Electron Spectrum α_1	α_2	p_b (MeV/c)
1	1980 Jun 29	10:41:40	3.55 ± 0.43	1.97	0.55	34.7	11.10	4.97	2.29
2	1980 Nov 12	04:48:32	3.67 ± 0.26	1.95	0.51	15.4	11.34	4.95	2.15
3	1981 Feb 17	21:46:02	3.53 ± 0.20	1.89	0.71	10.1	11.06	4.89	2.83
4	1981 Feb 24	00:10:27	3.56 ± 0.36	1.96	0.54	23.7	11.12	4.96	2.25
5	1981 Mar 23	06:55:37	4.29 ± 0.40	2.30	0.44	60.8	12.58	5.30	1.91
6	1981 Apr 26	11:44:05	3.32 ± 0.04	2.22	0.99	16.5	10.64	5.22	3.78
7	1981 May 4	08:38:08	3.39 ± 0.23	2.03	0.71	11.8	10.78	5.03	2.83
8	1982 Jun 15	00:30:15	2.58 ± 0.06	1.84	1.47	14.4	9.16	4.84	5.39
9	1982 Nov 22	12:23:12	3.50 ± 0.22	1.76	0.75	27.1	11.00	4.76	2.97
10	1984 May 22	14:56:57	3.10 ± 0.16	2.22	0.94	6.14	10.20	5.22	3.61
11	1986 Oct 19	00:40:27	3.23 ± 0.10	2.22	0.92	5.74	10.46	5.22	3.54
12	1988 Nov 13	23:05:02	3.46 ± 0.33	2.11	0.53	19.8	10.92	5.11	2.22
13	1989 Mar 7	05:57:27	4.70 ± 0.11	2.11	0.64	71.2	13.40	5.11	2.59
14	1989 Mar 7	13:18:19	3.04 ± 0.05	2.38	1.51	10.5	10.08	5.38	5.52
15	1989 Mar 7	14:51:58	3.60 ± 0.14	2.19	0.79	9.63	11.20	5.19	3.10
16	1989 May 4	11:13:15	3.30 ± 0.17	2.22	0.72	14.1	10.60	5.22	2.87
17	1989 May 6	17:01:02	2.85 ± 0.81	2.09	1.62	3.66	9.70	5.09	5.89
18	1989 Jun 16	07:38:29	3.57 ± 0.35	2.05	0.60	17.7	11.14	5.05	2.46
19	1989 Jul 20	20:26:59	2.92 ± 0.35	1.73	0.63	11.8	9.84	4.73	2.56
20	1989 Sep 5	22:22:26	3.75 ± 0.19	1.56	0.73	22.1	11.50	4.56	2.90
21	1989 Oct 24	19:15:59	3.19 ± 0.21	1.70	0.81	3.66	10.38	4.70	3.17
22	1989 Oct 27	11:30:51	3.77 ± 0.08	2.23	0.69	35.5	11.54	5.23	2.76
23	1989 Oct 27	19:00:11	3.69 ± 0.29	1.98	0.50	49.7	11.38	4.98	2.12

In Section 2, we first survey 15 spectral hardening events that were studied previously in the literature. We then perform a systematic examination of 185 flares from the *Solar Maximum Mission* (*SMM*; Vestrand et al. 1999). We identify a total of 23 electron-dominated events from the catalog of Vestrand et al. (1999) that show clear hardenings. For every one of these events, the break energy ε_b and the spectral indices below and above the break γ_1 and γ_2 are obtained. Assuming a thick target model (Brown 1971), the corresponding spectral indices and break energy for the source electrons are also obtained. We show that there is a clear anti-correlation between ε_b and γ_1. Discussions of the observations and how they fit into the scenario proposed by Li et al. (2013) are given in Section 3.

2. EVENT SELECTION AND DATA ANALYSIS

2.1. Review of Spectral Hardening Events

In Table 1, we list the spectral hardening events that have already been studied previously in the literature. Columns 1, 2, 6, and 8 give the event number, the date, the spacecraft/satellite, and the reference paper. Columns 3–5 are the flare spectrum parameters obtained from the references, i.e., the spectral indices before and after the break γ_1 and γ_2 and the break energy ε_b. In column 7, "Y" and "N" denote whether the event is electron-dominated. For events 1–6, this column is empty due to limited information given in the reference. The symbol "–" denotes "the same as above."

For Event 2, although Suri et al. (1975) suggested that the data above 700 keV were best described by an exponential rather than a power law, we chose the spectral index obtained from a power-law fit as γ_2.

Event 7 was reported by Trottet et al. (1998). These authors did spectral analysis for a total of six peaks (a–f) determined in count-rate temporal profiles and the count spectrum accumulated over the whole event ("S" in Table 2 in Trottet et al. 1998). For peaks c, d, e, and "S," when significant emission >1 MeV was detected, the spectra were fit with a double power law. It can be seen that all three peaks and "S" show a hardening behavior. The spectral shapes of peaks c and e are similar, while in peak d the break energy ε_b is much larger and the spectrum is harder (both γ_1 and γ_2 are smaller). As shown below, these results agree with our statistical result that γ_1 is anti-correlated with ε_b.

Events 11–13 were observed by a γ-ray detector on *RHESSI* (Lin et al. 2002) and Event 14 was observed by *Fermi* (Ackermann et al. 2012). In these four events, the contribution of γ-ray lines, which is not non-negligible, has to be removed in order to obtain the electron Bremsstrahlung component. Note that for Event 13, γ_1 and γ_2 listed in Table 1 are the spectral indices of the combined footpoint sources and the coronal source; $\varepsilon_b \sim 0.45$ MeV is determined from the intersection of the two spectral lines (see Figure 3 in Krucker et al. 2008). For Event 14, $\varepsilon_b \sim 1.3$ MeV is determined from the intersection of the two power-law curves (see Figure 3 in Ackermann et al. 2012).

Event 15 is from Rieger et al. (1998) and it is a composite event of 10 electron-dominated episodes or events recorded by the Gamma-Ray Spectrometer (GRS) on *SMM*. The values $\gamma_1 \sim 2.73$ and $\gamma_2 \sim 1.84$ are the median values of the 10 events/episodes. In Rieger et al. (1998), the break energy was assumed to be 1 MeV for all 10 events/episodes; we adopt a different procedure below.

2.2. Events from SMM Observations

Vestrand et al. (1999) listed a total of 258 γ-ray flares detected at energies above 300 keV by *SMM*/GRS during the period from 1980 February to 1989 November. These authors also presented an atlas of energy spectra for 185 flares that were intense enough to permit spectral analysis.

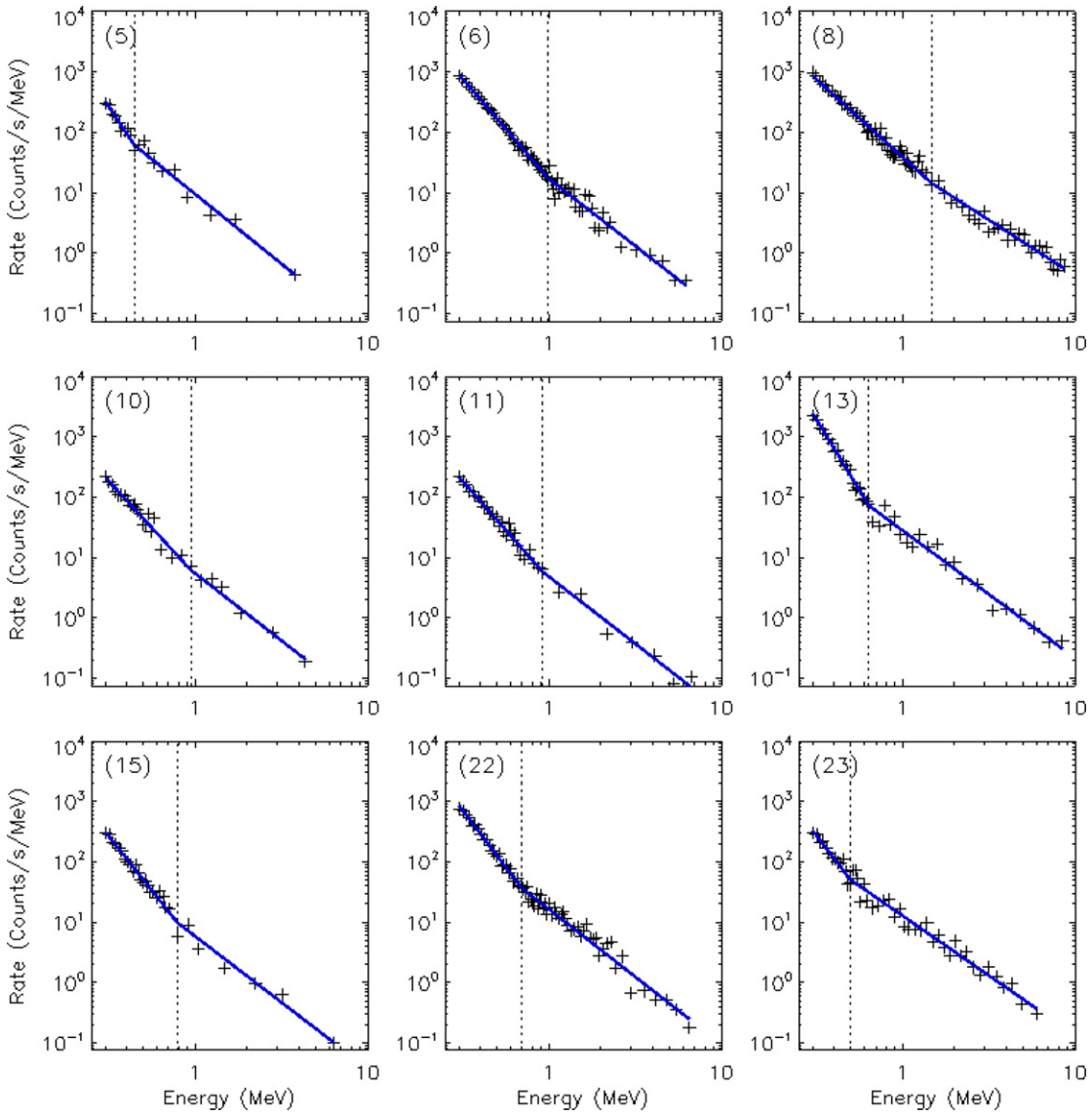

Figure 1. Nine example events from Table 2.
(A color version of this figure is available in the online journal.)

From these 185 events, we identified 118 flares that have no strong nuclear components. Among these, 23 events show clear spectral hardening and they are listed in Table 2. Columns 1–3 show the event number, the date, and the approximate time of the onset emission above 300 keV (i.e., column 2 in Table 1 of Vestrand et al. 1999).

For the episodes or events studied in Rieger et al. (1998), we only include the 1982 June 15 event in Table 2. The reasons for this are as follows. (1) The first event in Rieger et al. (1998) was also studied by Dennis (1988) and is listed in Table 1. Its spectrum clearly hardens at ∼0.3 MeV and does not show obvious hardening (>0.3 MeV) in the figure in Vestrand et al. (1999). (2) No spectral plot for the sixth event in Rieger et al. (1998) is provided in Vestrand et al. (1999). (3) The spectral plots of the remaining events provided in Vestrand et al. (1999) show a significant nuclear component even though they were regarded as "electron-dominated" in Rieger et al. (1998), which may be due to the fact that different time intervals were used. So, these events do not agree with our selection criteria.

For fitting purposes, the background-subtracted count rate spectrum for each γ-ray flare event is reproduced by extracting the data points directly from the online gif plots provided on the SMM Web site (ftp://umbra.nascom.nasa.gov/pub/smm/smmgrs/rate_plots/). In order to proceed efficiently, we ignore the error bars and channel widths in this process.

Nine examples are shown in Figure 1. We fit each event with a double power law in the following way. We first estimate a break energy ε_b. Then, the power spectrum before the break, plotted in logarithmic coordinates, is fit by a least-squares polynomial linear fit using the IDL function *POLY_FIT*. *POLY_FIT* also returns the 1σ error estimate. For the power spectrum above the break, the slope (i.e., γ_2) is calculated by the least-squares method

$$\gamma_2 = \frac{\sum_i (y_i - y_0)(x_i - x_0)}{\sum_i (x_i - x_0)^2},$$

where x_0 is the break energy and y_0 is the corresponding count rate obtained from the linearly fitted spectrum before the break; (x_i, y_i) are the coordinates of the data points above the break.

The break energy ε_b is then varied within a small range until we obtain the smallest 1σ error. The fitted photon spectrum parameters γ_1, and its 1σ error, γ_2, and ε_b are listed in columns

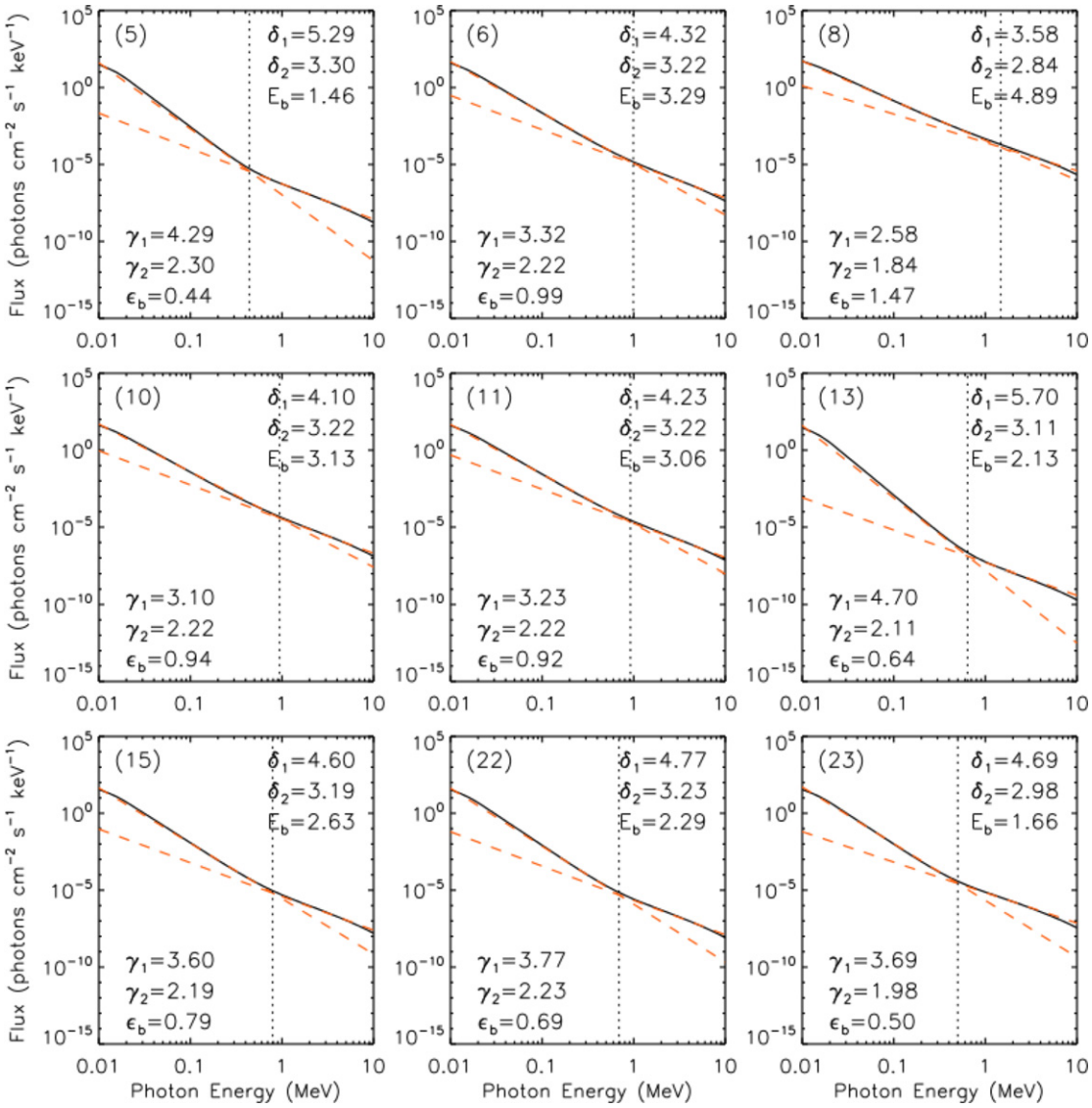

Figure 2. Photon spectra deduced from the source electron spectra with $\delta_1 = \gamma_1 + 1$, $\delta_2 = \gamma_2 + 1$, and $E_b \sim 3.33\varepsilon_b$ for the events shown in Figure 1. In fitting the spectra, the low- and high-energy cutoffs are set to $E_{\rm LC} = 20$ keV and $E_{\rm HC} = 32$ MeV, respectively.

(A color version of this figure is available in the online journal.)

4–6 in Table 2. $N(\varepsilon_b)$, the count at the break energy, is listed in column 7 of Table 2.

One can obtain the corresponding source electron current $j(E)$ from the continuum photon spectrum. We assume that $j(E)$ is also described by a broken power law such that $j(E) \sim E^{-\delta_1}$ when $E < E_b$ and $j(E) \sim E^{-\delta_2}$ when $E > E_b$. In relating δ_i to γ_i ($i = 1, 2$), two models frequently used are the thick target and the thin target model. Considering the thick target model (Brown 1971) as an example, we have $\delta_2 = \gamma_2 + 1$ and, as a crude simplification, $\delta_1 = \gamma_1 + 1$ (since electrons above the break also generate HXR photons below the break). To determine E_b, we used the IDL program *brm2_ThickTarget.PRO* in Object Spectral Executive (OSPEX) and varied E_b until we obtained the best fit to the photon spectrum.

Figure 2 shows the photon spectrum calculated for a given electron current $j(E)$ for the nine events shown in Figure 1. The two dashed lines are the fitted spectra below and above the break energy ε_b (i.e., γ_1 and γ_2). In using the fitting program, since we are only interested in HXR spectra, which are constrained to be above >20 keV in solar flares, we set the low- and high-energy cutoffs to be $E_{\rm LC} = 20$ keV and $E_{\rm HC} = 32$ MeV. We also set the total electron flux $F_0 = 10^{35}$ s^{-1}. Note that we do not fit the absolute value of the photon flux in Figure 1 as we are only interested in the shape of the photon spectrum.

For most events in Table 2, we find that the break energy of the source electron satisfies $E_b \sim 3.33\varepsilon_b$. From $j(E)$, one can obtain the distribution function $f(p)$ of the source electron through the relationship $j(E) = p^2 f(p)$. Let $f(p) \sim p^{-\alpha_1} H(p_b - p) + p^{-\alpha_2} H(p - p_b)$, where H is the Heaviside function, and assuming that α_1 and α_2 are given by p in the non-relativistic and the relativistic limits, respectively, then we have:

$$\alpha_1 = 2(\gamma_1 + 1) + 2, \quad \alpha_2 = (\gamma_2 + 1) + 2, \text{ and}$$
$$p_b = \sqrt{E_b(E_b + 2m_e c^2)}/c.$$

The parameters α_1, α_2, and p_b of the electron spectrum are listed in columns 8–10 in Table 2 and can be compared directly with numerical simulation results (e.g., Li et al. 2013). Note that p_b listed here should be equivalent to p_m in Li et al. (2013).

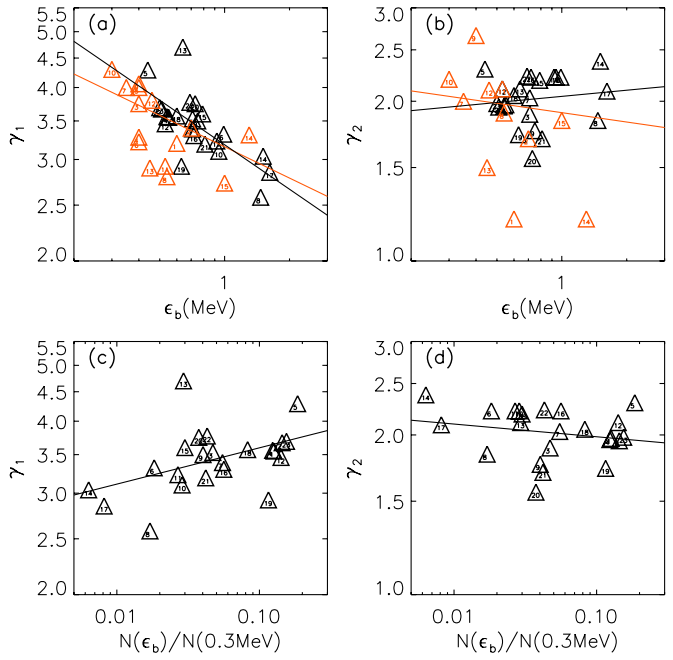

Figure 3. (a) Correlation between γ_1 and the break energy ε_b. Events in Table 1 are marked with red triangles and events in Table 2 are marked with black triangles, with the event numbers indicated inside the triangles. Panel (b) is the same as panel (a), but for the correlation between γ_2 and the break energy ε_b. (c) Correlation between γ_1 and $N(\varepsilon_b)/N(0.3\ \mathrm{MeV})$. (d) Correlation between γ_2 and $N(\varepsilon_b)/N(0.3\ \mathrm{MeV})$.

(A color version of this figure is available in the online journal.)

This p_m was found to be two to three times larger than the break momentum in the expression of β_s, as shown in Figure 1 of Li et al. (2013).

2.3. Statistical Results

Figure 3 shows the correlation of γ_1 (γ_2) with both the break energy ε_b and the normalized counts, which are defined as $N(\varepsilon_b)/N(0.3\ \mathrm{MeV})$.

In Figures 3(a) and (b), the flare spectral indices γ_1 and γ_2 are plotted as a function of the break energy ε_b. Events in Table 1 are marked with red triangles and events in Table 2 are marked with black triangles, with the event numbers indicated inside the triangles. For Events 3–6 in Table 1, there were no γ_2s. So, these events are not shown in Figure 3(b). For Event 7 in Table 1, we use the parameters of the accumulated spectrum over the whole event "S"; for Event 8 in Table 1, we only use *GRANAT* data.

For the 38 events that have γ_1 measurements, all but one are in the range of 2.5–4.5. For the 34 events that have γ_2 measurements, 31 of them are in the range of 1.5–2.5. In seven events, we have $\gamma_1 - \gamma_2 \gtrsim 2$. As noted in Dennis (1988) and Kontar et al. (2007), spectral breaks as large as 2 are hard to explain by merely including electron–electron Bremsstrahlung or relativistic corrections for the electron–nucleon cross section.

To better understand the relationship between γ_1 (γ_2) and ε_b, we conduct a linear regression fit using the IDL function *REGRESS* (with ε_b in logarithmic coordinates) in Figure 3. In panels (a) and (b), the black lines are obtained from events in Table 2 (black triangles). These events are obtained from *SMM* only and do not have calibration issues. The slopes of the two fits are -0.257 and 0.038 and the correlation coefficients are -0.709 and 0.126. These correlation coefficients indicate that γ_1 strongly anti-correlates with ε_b, while γ_2 does not appear to correlate with ε_b. If we consider all events from both Tables 1 and 2 together, then the fits are given by the red lines. The slopes are -0.181 and -0.059 and the correlation coefficients are -0.557 and -0.138. Clearly, since the events in Table 1 come from multiple spacecraft/instruments, the correlation for the entire set is considerably weakened.

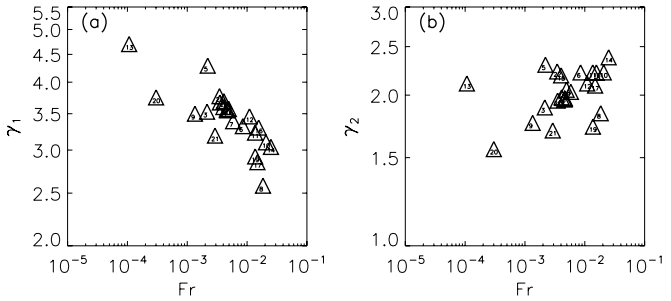

Figure 4. (a) Correlation between γ_1 and the fraction Fr of photons that are above the break. (b) Correlation between γ_2 and the fraction Fr of photons that are above the break.

In Figures 3(c) and (d), the flare spectral indices γ_1 and γ_2 are plotted as a function of $R = N(\varepsilon_b)/N(0.3\ \mathrm{MeV})$, which is the ratio of counts at ε_b to the counts at 0.3 MeV. To minimize possible instrumental uncertainties, only events from *SMM* are examined. Note that for a power-law spectrum, $N(\varepsilon_b)/N(0.3\ \mathrm{MeV})$ is fully determined when γ_1 and ε_b are given. So, a correlation between γ_1 and ε_b implies a correlation between γ_1 and R. From both panels (a) and (c), we see that Events 8, 13, and 19 seem to be outliers. A further detailed investigation of these three events may be important to understanding the underlying mechanism causing the spectral break.

One can also examine the correlation between γ_1 (γ_2) and the fraction Fr of photons above the break to the total photons. The latter is defined as:

$$\mathrm{Fr} = \frac{\int_{\varepsilon_b}^{10\,\mathrm{MeV}} N(\varepsilon)d\varepsilon}{\int_{20\,\mathrm{keV}}^{10\,\mathrm{MeV}} N(\varepsilon)d\varepsilon}. \quad (1)$$

If the break is caused by two different spectra, for example, spectra that are from two different spatial locations (footpoints and looptops), then we expect that Fr will depend on how much occulation is in the event. Consequently, it is unlikely that there will be a correlation between γ_1 and Fr. If, however, the break is due to the hardening of a single power law, then we expect to recover an anti-correlation between γ_1 and Fr. Figure 4 plots the correlation between γ_1 (γ_2) and Fr. As one can see, γ_1 and Fr appear to be anti-correlated. Indeed, for a linear fit of γ_1 versus ln(Fr), the correlation coefficient is -0.791. Note, however, because Fr is mostly sensitive to the number of photons at low energies, the choice of the low-energy cutoff, 20 keV, as used in Equation (1), can affect the correlation. So, caution must be taken when interpreting Figure 4.

3. DISCUSSION

In our recent work, Li et al. (2013) proposed a scenario for spectral hardening in flare continuum emission based on diffusive shock acceleration of electrons at a finite-width flare termination shock. In this scenario, the intensity of the turbulence $I(k)$ determines the magnitude of the diffusion coefficient κ, which in turn controls whether spectral hardening will occur. At low energies ($p < p_b$), electrons resonate with the dissipation range turbulence and κ has a very shallow dependence on electron momentum, which results in a power-law spectrum below

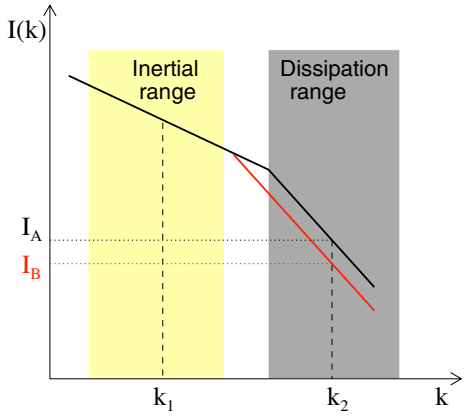

Figure 5. Schematic of the flare site turbulence spectra for two flares A and B that only differ with respect to the location where the dissipation range sets in. (A color version of this figure is available in the online journal.)

the break. At high energies ($p > p_b$), electrons resonate with the inertial range turbulence and κ has a strong dependence on electron momentum, so β_s increases rapidly to a value much larger than unity. The spectrum above the break can therefore also be approximately fit by a power law. As a result, we observe a broken spectrum with hardening at high energies.

The anti-correlation between γ_1 and ε_b from this study can be shown to be a consequence of the scenario discussed in Li et al. (2013). To see why, consider two nearly identical flares A and B that only differ in their turbulence spectra, as shown in Figure 5. Assuming that flare A has a larger k_b than flare B, then the corresponding turbulence level $I(k)$ at a k_2 in the dissipation range ($k > k_b$) is larger for flare A, i.e., $I_A(k_2) > I_B(k_2)$. Since the spectral index α_1 at a momentum p that resonates with k_2 is proportional to $I(k_2)$ (Li et al. 2013), we therefore have $\alpha_1(A) > \alpha_1(B)$. In comparison, for a k_1 in the inertial range, we have $I_A(k_1) = I_B(k_1)$, so $\alpha_2(A) = \alpha_2(B)$.

Because $k_b(A) > k_b(B)$, we also have $p_b(A) < p_b(B)$. Therefore, the scenario proposed by Li et al. (2013) implies that α_1 and p_b are anti-correlated. This result is what is shown in Figure 3. Note that it has been argued that the length scale when the inertial range transitions into the dissipation range is the thermal proton Larmor radius $\sim ((\sqrt{k_B T/m_p})/\Omega_p)$ (Leamon et al. 1998, 1999). In this case, the p_b of the electron spectrum is dictated by the kinetic energy of thermal protons and flare A in our example therefore has a lower temperature than flare B.

The lack of a correlation between γ_2 and ε_b can also be explained. For the spectrum above the break, electrons resonate in the inertial range where their diffusion coefficient increases rapidly with energy (the associated β_s, as defined in Equation (3) of Li et al. 2013 increases rapidly to >1). In such a case, Li et al. (2013) showed that α_2 is largely dictated by the shock compression ratio s, i.e., $\alpha_2 \sim 3s/(s-1)$. If flares A and B have a similar compression ratio, then their γ_2 values will not differ much. As a result, γ_2 does not exhibit a good correlation with ε_b. Furthermore, the shock compression ratio can be inferred from the range of γ_2. For example, for a range of γ_2 between 1.5 and 2.5, with the thick-target model, we can obtain $s \sim 2.2$–3.0 (Li et al. 2013). Considering the contribution of the $1/\beta_s$ term to α (Equation (2) of Li et al. 2013), s should be somewhat larger than this estimated value.

Note that in our study, we only selected 23 spectral hardening events from the 258 γ-ray flares from Vestrand et al. (1999). The selection was partly affected by the fact that the lower energy end of the spectra in Vestrand et al. (1999) was close to 300 keV. Obviously, events that show hardening at lower energies will be ignored. In a future work, we plan to combine data of Hard X-Ray Burst Spectrometer (HXRBS) and GRS on *SMM* to search for more spectral hardening events that show breaks at energies below or around 300 keV, similar to Figure 18 in Dennis (1988).

Finally, we note that there are other proposals for the observed hardening of the continuum spectrum. Some of these proposals have been discussed in the previous sections. Perhaps the most important difference between our proposal and other proposals is that ours advocates that the continuum spectrum is a *single* spectrum and that the hardening reflects an intrinsic hardening of the source electrons. Because the spectrum is due to a single source, it cannot be a sum of two or more spectra from different spatial locations. This realization allows us to differentiate our scenario from others by examining, for example, partially occulted flares and the time evolution of the spectrum. Such studies will be explored in the future.

Furthermore, we have only considered electron-dominated events. In nuclear line-dominated events, hardening may well exist. However, it is important that we subtract the contributions from individual nuclear lines (G. H. Share 2012, private communication). The remaining electron Bremsstrahlung component may exhibit hardening at high energies (Share & Murphy 2006). Extending our analyses to γ-ray flare events, including those observed by recent missions such as *RHESSI* and *Fermi*, which have higher temporal and energy resolution, will also be pursued.

We gratefully acknowledge Dr. Gordon Holman's group for developing and making public the IDL codes used here for the Bremsstrahlung calculations. We thank the referee for many useful comments and suggestions; in particular, the suggestion for producing Figure 4. This work is supported in part by NSF grants ATM-0847719, AGS0962658, and AGS1135432 at UAHuntsville and the 973 Program No. 2012CB825601 and NNSFC grant Nos. 41274175 and 41028004 at SDUWH. X.L.K. acknowledges financial support by the Shandong University Graduate Study Abroad Fund.

REFERENCES

Ackermann, M., Ajello, M., Allafort, A., et al. 2012, ApJ, 745, 144
Asai, A., Kiyohara, J., Takasaki, H., et al. 2013, ApJ, 763, 87
Brown, J. C. 1971, SoPh, 18, 489
Aschwanden, M. J. 2004, Physics of the Solar Corona: An Introduction (Berlin: Springer), Chap. 14
Chen, B., & Bastian, 2012, ApJ, 750, 35
Dennis, B. 1988, SoPh, 118, 49
Fletcher, L., Dennis, B. R., Hudson, H. S., et al. 2011, SSRv, 159, 19
Gruber, D. E., Peterson, L. E., & Vette, J. I. 1973, in High Energy Phenomena on the Sun, ed. R. Ramaty & R. G. Stone (NASA SP-342; Washington, DC: NASA), 147
Holman, G. D., Aschwanden, M. J., Aurass, H., et al. 2011, SSRv, 159, 107
Kawate, T., Nishizuka, N., Oi, A., Ohyama, M., & Nakajima, H. 2012, ApJ, 747, 131
Kontar, E. P., Brown, J. C., Emslie, A. G., et al. 2011, SSRv, 159, 301
Kontar, E. P., Emslie, A. G., Massone, A. M., et al. 2007, ApJ, 670, 857
Krucker, S., Hudson, H. S., Glesener, L., et al. 2010, ApJ, 714, 1108
Krucker, S., Hurford, G. J., MacKinnon, A. L., Shih, A. Y., & Lin, R. P. 2008, ApJL, 678, L63
Li, G., Kong, X. L., Zank, G., & Chen, Y. 2013, ApJ, 769, 22
Li, G., Zank, G. P., Verkhoglyadova, O., et al. 2009, ApJ, 702, 998
Leamon, R. J., Smith, C. W., Ness, N. F., Matthaeus, W. H., & Wong, H. K. 1998, JGR, 103, 4775
Leamon, R. J., Smith, C. W., Ness, N. F., & Wong, H. K. 1999, JGR, 104, 22331

Lin, R. P. 2011, SSRv, 159, 421
Lin, R. P., Dennis, B. R., Hurford, G. J., et al. 2002, SoPh, 210, 3
Lin, R. P., Krucker, S., Hurford, G. J., et al. 2003, ApJL, 595, L69
Moses, D., Droge, W., Meyer, P., & Evenson, P. 1989, ApJ, 346, 523
Park, B. T., Petrosian, V., & Schwartz, R. A. 1997, ApJ, 489, 358
Rieger, E., Gan, W. Q., & Marschhäuser, H. 1998, SoPh, 183, 123
Rieger, E., & Marschhäuser, H. 1990, in Proc. Third Max '91 Workshop, ed. R. M. Wingler & A. L. Kiplinger (Boulder, CO: Univ. Colorado), 68
Share, G. H., & Murphy, R. J. 2006, Solar Eruptions and Energetic Particles, ed. N. Gopalswamy, R. Mewaldt, & J. Torsti (Geophys. Monogr. Ser., Vol. 165; Washington, DC: AGU), 177
Share, G. H., Murphy, R. J., Skibo, J. G., et al. 2003, ApJL, 595, L85
Shih, A. Y., Lin, R. P., & Smith, D. M. 2009, ApJL, 698, L152
Silva, A. V. R., Wang, H., & Gary, D. E. 2000, ApJ, 545, 1116
Suri, A. N., Chupp, E. L., Forrest, D. J., & Reppin, C. 1975, SoPh, 43, 415
Trottet, G., Vilmer, N., Barat, C., et al. 1998, A&A, 334, 1099
Vestrand, W. T. 1988, SoPh, 118, 95
Vestrand, W. T., Share, G. H., Murphy, R. J., et al. 1999, ApJS, 120, 409
Vilmer, N., Mackinnon, A. L., & Hurford, G. J. 2011, SSRv, 159, 167
Vilmer, N., Trottet, G., Barat, C., et al. 1999, A&A, 342, 575
Yoshimori, M., Takai, Y., Morimoto, K., Suga, K., & Ohki, K. 1992, PASJ, 44, L107
Yoshimori, M., Watanabe, H., & Nitta, N. 1985, JPSJ, 54, 4462